Struct Chem (2014) 25:1711–1723
DOI 10.1007/s11224-014-0454-y

ORIGINAL RESEARCH

β-Nitroso-*o*-quinone methides: potent intermediates in organic chemistry and biology. The impact of the NO group on their structure and reactivity profile: a theoretical insight

Paweł Kozielewicz · Petros G. Tsoungas · Demeter Tzeli · Ioannis D. Petsalakis · Mire Zloh

Received: 27 February 2014 / Accepted: 5 April 2014 / Published online: 31 May 2014

Abstract The structure and reactivity profiles of prototype *o*-quinone methides **1**, **2** and their β-nitroso analogues **6–9** have been investigated by means of DFT and MP2 calculations. These highly reactive unstable species are generated by oxidative dearomatization of their precursor oximes. The destabilization of their structure is more pronounced in the β-nitroso congeners **7–9**. There is only a weak π conjugation across the nitrosoalkene arm. The latter gives rise to *E* and *Z* conformations and causes some distortion on the ring σ-frame, while the π-frame is weakly perturbed. The *Z* conformation is the most stable in all structures. Their geometry is also affected by the *o*-quinone ring and the 1,2-(**7** and **8**) and 2,3-(**9**) isomer pattern. The stability of these conformations is rationalized in terms of *ortho*- or *peri*- ring formations. The impact of their geometry profile on their reactivity pattern has been studied by means of reactivity descriptors such as Fukui and Parr functions, chemical potential and hardness, HOMO and LUMO energies and their separation (HOMO–LUMO gap) as well as aromaticity indices such as HOMA and out-of-plane deformability. All descriptors consistently demonstrate that the reactivity is dominated by an *E*/*Z*-controlled intramolecular *ortho*- or *peri*-cyclization mode to fused 1,2-oxazoles or 1,2-oxazines vs indoles, respectively. Intermolecular primary reactions can occur at the quinone alkene bond or that of the nitrosoalkene arm.

Keywords β-Nitroso-*o*-quinone methides · DFT calculations · Intramolecular cyclization · Oxazoles · Indoles · Intermolecular reactions

Electronic supplementary material The online version of this article (doi:10.1007/s11224-014-0454-y) contains supplementary material, which is available to authorized users.

P. Kozielewicz
School of Clinical and Experimental Medicine, University of Birmingham, Edgbaston, Birmingham B15 2TT, UK

P. Kozielewicz
Faculty of Pharmacy, Medical University of Warsaw, Banacha 1, 02-097 Warsaw, Poland

P. G. Tsoungas (✉)
Department of Biochemistry, Hellenic Pasteur Institute, 127 Vas.Sofias Ave., Athens 11510, Greece
e-mail: pgt@pasteur.gr

D. Tzeli · I. D. Petsalakis
Theoretical and Physical Chemistry Institute, National Hellenic Research Foundation, 48 Vassileos Constantinou Ave., Athens 116 35, Greece

M. Zloh
UCL School of Pharmacy, University College London, 29-39 Brunswick Square, London WC1 1AX, UK

M. Zloh
Department of Pharmacy, University of Hertfordshire, College Lane, Hatfield AL10 9AB, UK

Introduction

o-Quinone methide prototypes **1** and **2** are ubiquitous in chemistry and biology (Fig. 1) [1, 2]. They have enjoyed attention as reactive intermediates in organic and bioorganic synthesis. The widespread interest in their chemistry, during the last two decades, has been fueled by their significance in biological processes and drugs [1]. Lately, there has been a resurgence of interest in their chemistry [3, 4] and biology [5, 6].

It has been suggested that **1** plays a key role in the chemistry of several classes of antibiotics and antitumour drugs such as mitomycin C [7, 8] and anthracyclines

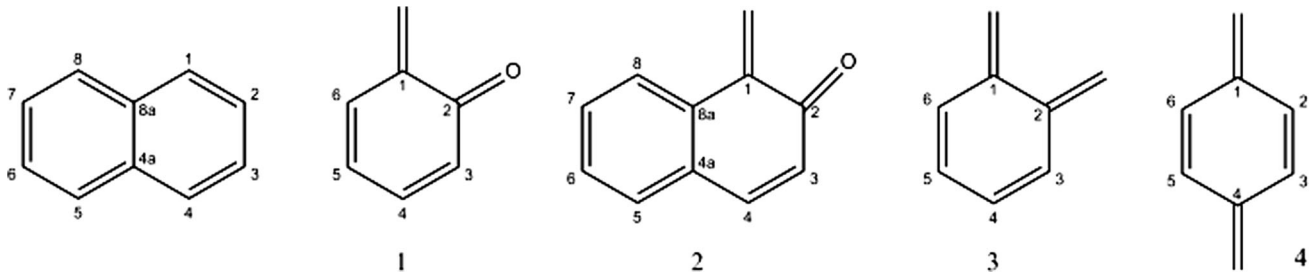

Fig. 1 Structures of naphthalene, *o*-quinone methides **1**, **2** and *o*-, *p*-quinodimethanes **3**, **4**

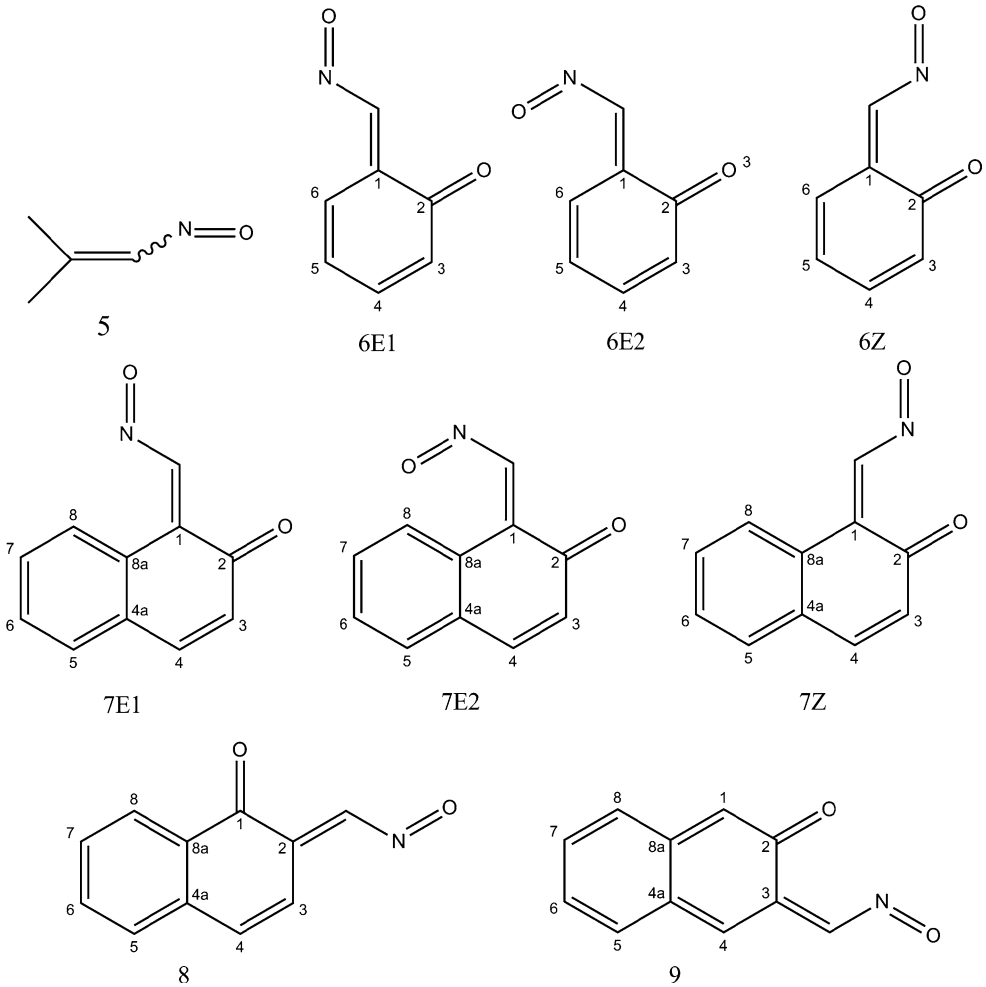

Fig. 2 β-Nitrosoalkene **5** and β-nitroso-*o*-quinone methides **6** and **7**–**9** (the spatial arrangement of NO group is designated as *Z*- or *E*-conformation if it is towards the carbonyl O atom or away from it, respectively. The *E*-conformation is distinguished as E_1 or E_2 if the O atom of NO is away from or towards the ring)

[9–11]. Its pronounced biological activity rests largely upon its mode of action on cellular macromolecules. It has been found that it can be involved in cross-linking of ligands with nucleic bases, peptides, or proteins [12, 13] and as such it can be implicated in biomolecular applications [14–16].

The polar nature of **1** or **2** endows them with electrophilic and nucleophilic reactivity. Thus, as highly polarized species, they react with electrophiles [17–20] and nucleophiles [21, 22]. The latter is the most commonly used, and it is usually driven by the rearomatization of the structure. DFT calculations have been reported with sulphur, nitrogen, and oxygen nucleophiles [23]. **1** or **2** are related to *o*-quinonedimethanes **3** [24, 25] and *p*-quinone methides **4** [26] (Fig. 1). Unlike **4**, **1** (or **2**) cannot be easily isolated. Therefore, it is commonly trapped in situ by (Hetero) Diels–Alder reactions, where **1** acts as a (hetero) diene [27, 28]. Early computational studies on the parent structure **1** [1, 2] as well as some recent DFT-based ones [29, 30] have focused on deciphering its reactivity as a Diels–Alder

component or its biological activity as a Michael acceptor, in aqueous media [21, 31–33].

Conjugated β-nitrosoalkenes **5** [16, 34–38] (Fig. 2) constitute a well-known class of reactive molecules. They have been identified by isolation (in some cases, at least) [39], spectroscopic characterization [40] or studies of their kinetics and stereochemistry [41]. Their stability increases markedly by halogen, aryl or *t*-alkyl substituents as well as upon strong intramolecular H-bonding [42] or formation of transition metal complexes [43]. These molecules are trapped by reactions similar to those of **1** [34–38]. A species closely related to both **1** (or **2**) and **5** is β-nitroso-*o*-quinone methides **6** or **7**–**9** (Fig. 2). This has been proposed in our earlier reports as being transiently generated during the oxidation of *o*-hydroxyaryl acyloximes [44–47]. The nitrosoalkene motif has been extensively studied in the N-oxide chemistry of furazans [44, 45] and has also been invoked in the formation of N-oxides of 1,2-benzisoxazoles [44–47].

Experimental findings from our investigations [22, 44–47], already reported or in progress, point to intriguing aspects of the structures **1** and **6**–**9**. Thus, in the absence of a reaction partner (trapping dienophile or nucleophile), the intramolecular *o*- and *peri*-cyclizations of **6** or **7** are the only reactions observed [46, 47]. Interestingly, this is the primary reaction course still taken, even in the presence of a nucleophile [48].

o-Quinone methides **2** and **7** have been engaged in Diels–Alder cycloaddition, acting either as dienophiles [22] or as both dienes and dienophiles [46, 47]. Preliminary experiments have also shown that the *o*-quinone ring double bond behaves as an isolated typical alkene, undergoing electrophilic addition at C-3 [49]. Heterocycles with a ring N–O bond are important core structures in many pharmaceutics. Among them, the isoxazole ring occupies a prominent position in isoxazole-based marketed drugs, such as, for example, penicillin antibiotics (cloxacillin, dicloxacillin, flucloxacillin), antipsychotic (risperidone, paliperidone), COX 2 inhibitors (parecoxib) to name a few.

Structures **6** or **7** are key intermediates in the formation of many of these compounds. Arene-fused 1,2-oxazoles (mainly benzisoxazoles) that are C-3 substituted with pharmacophores is an area of intense research driven by diverse pharmaceutical applications [50]. Furthermore, ring opening of these heterocycles, asymmetric reduction in particular, provides access to optically active structures, core components in a variety of medicines [51].

The chemistry and multifaceted significance of **1** and **2**, the potential of **6**–**9** as intermediates in organic or bioorganic synthesis [1–3], as outlined above, particularly towards diverse-substituted arene-fused isoxazoles or 1,2-oxazines, sparked the present theoretical insight into the salient features of these intermediates, the first systematic study of this species while a reflection on their expected reactivity pattern is described.

Table 1 Relative energy levels (kcal mol^{-1}) of the calculated minima and transition states for **7** → *peri*-cyclization product (P) calculated at different levels of theory

	$7E_1$ → TS_2			TS_3 → product (P)		
	$7E_1$	TS_1	TS_2	TS_3	TS_4	(P)
B3LYP/6−311+G**	0	8.3	−4.5	0	56.6	−14.4
B3LYP/aug-cc-pVTZ	0	8.1	−5.2	0	58.1	−16.0
M062X/6−311+G**	0	13.5	−8.2	0	58.9	−13.9
M062X/aug-cc-pVTZ	0	13.1	−9.0	0	57.2	−15.9
MP2/6−311+G**	0	7.3	−3.6	0	56.7	−12.9

Methodology

Ab initio DFT and MP2 calculations have been performed to carry out full geometry optimization and compute the energies of the target molecules. The unrestricted B3LYP functional were employed in conjunction with the 6−31G** and 6−311++G** basis sets, and the second-order Møller-Plesset Perturbation Theory (MP2) were used in conjunction with the 6–311++G** basis set in order to evaluate the impact of dearomatization of oximes I and the conformation (*Z* or *E*) of the NO group on the resultant *o*-quinone methide structures III.

The performance of the B3LYP functional, despite its widely accepted popularity, has been questioned [52, 53] underestimation of barrier heights being one of the issues raised. Thus, to increase the credibility of our findings, this functional has also been used with the aug-cc-pVTZ [54] basis set whereas the M06-2X hybrid meta functional [52] has also been called in and used with both 6−311+G** and aug-cc-pVTZ basis sets, too (Table 1). All methods resulted in similar geometries. Transition State (TS) energies derived from both basis sets of the same functionals have also been found to be similar. B3LYP and MP2 approaches have given comparable relative energies (Table S1, Supporting Information). A *ca.* 40 % higher energy barrier has, indeed, been calculated by the M06-2X functional (Table S1, Supporting Information). However, it should be pointed out that (a) the barriers in all cases have been still low and (b) all reaction and barrier energies, obtained by both functionals, have been ultimately found of comparable magnitude (Table S1). It is, therefore, safe to accept the reliability of our B3LYP-based calculations.

All calculations have been performed and visualized using NWChem [55], ECCE packages [56] and Spartan [57]. The results of each lower level were used as input for the higher theory calculations. Geometry-based parameters

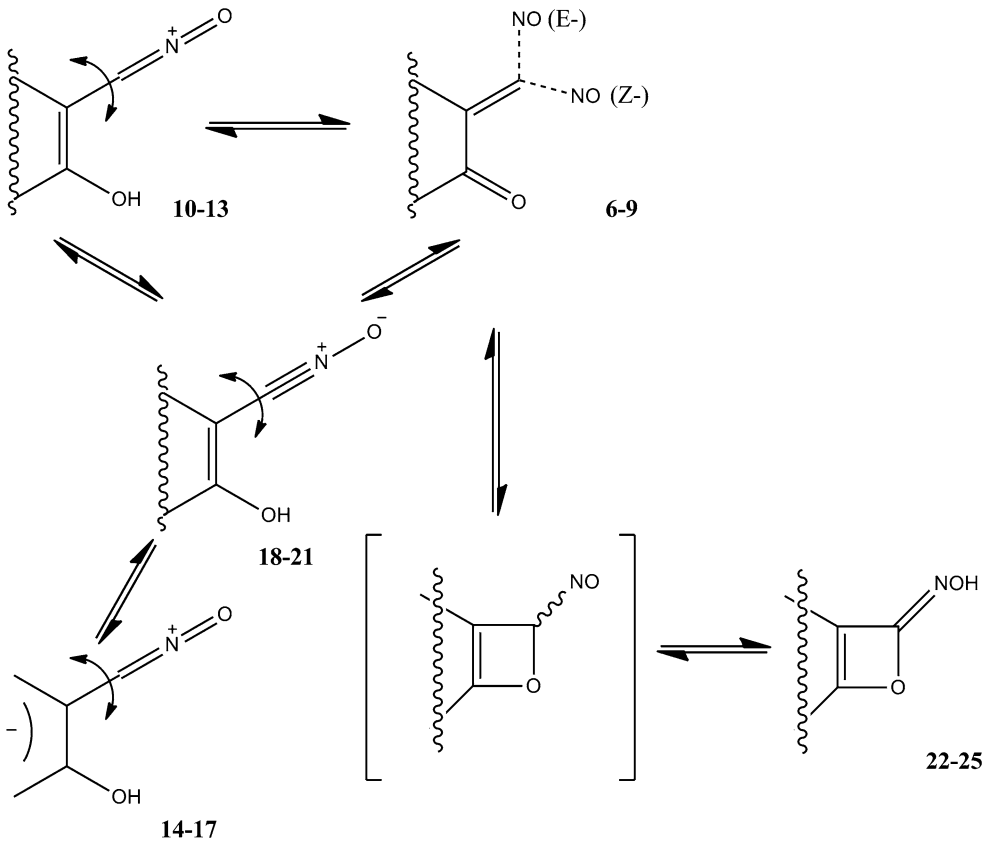

Fig. 3 H transfer-based or ring-chain interconversion of structures contributing to the identity of *o*-quinone methides **III** (**6–9**)

such as bond lengths, π-bond orders, total and relative energies, dihedral angles, dipole moments, reactivity descriptors such as charge densities, chemical potential μ, chemical hardness η, frontier orbital energies and aromaticity indices such as Harmonic Oscillator Model of Aromaticity (HOMA) and out-of-plane ring deformability (E_{def}) have been calculated to assess various features of the structures and predict the reactivity profile of **6** and **7–9**.

Although intramolecular cyclization (*ortho-* and *peri-*) appears to be the prevalent reactivity mode, it is the strongly polar (electrophilic) character of **6–9**, as depicted by formalisms **10–21** (Fig. 3), that called for the use of additional rigorous reactivity descriptors.

Condensed Fukui function f_{k} and the recently reported local electrophilicity and nucleophilicity indices ω_{k} and NK of Parr functions P(r) [58] have been chosen as such, to provide a more accurate, perhaps, estimate of their site selectivity towards nucleophiles and electrophiles. Parr functions were calculated at 6−31G* theory level as in the original work [58].

Chemical potential μ [59, 60] and hardness η [61, 62] are expressed in terms of ionization potential I and electron affinity A as $\mu = -(I + A)/2$ and $\eta = (I - A)/2$ (or $\eta = (E_{\text{LUMO}} - E_{\text{HOMO}})/2$), respectively. The HOMO–LUMO gap (energy separation) is known [63] to be related to stability, i.e. reactivity and this relationship has been theoretically articulated as hardness η.

Reformulated HOMA (rHOMA) index [62, 64] has been calculated by the delineated equation.

$$\text{rHOMA} = 1 - \frac{\propto}{n}\sum_{i=1}^{n}(R_{\text{opt}} - R_i)^2$$

$$\alpha_{\text{Cring–Cring}} = 257.7,\ R_{\text{opt}} = 1.388 \text{ for } C_{\text{ring}} - C_{\text{ring}}$$

where n is the number of bonds in the aromatic system ($n = 6$ for 1-ring, i.e. **6** and $n = 11$ for a 2-ring system, i.e. **7–9**). R_{opt} is the optimum bond length, and R_i is the real bond length of the i bond taken into consideration. This equation necessitates the use of the normalization constant α for each type of bond. In our case, there are no ring heteroatoms, therefore $\alpha = 257.7$.

π delocalization-related deformation energy (E_{def}) [65, 66] has been calculated as follows: torsion angles X for the optimized low energy conformation of the oxime and Y for the *o*-quinone methide structure have been calculated. Then, Y was constrained into X and the energy of the newly built conformation was calculated. The energy change upon constraining X and Y angles of the *o*-quinone methide gives the deformation energy E_{def}.

The Fukui function $f(r)$ [67–69] represents the response of μ of a system to an external potential change and it is expressed (in its condensed form) as $f_k^+ = [q_k\ (N+1) - q(N)]$ or $f_k^- = [q_k\ (N) - q_k(N-1)$ or $f_k = [q_k(N+1) - q_k(N-1]/2$ (where q_k is the electron population of an atom k and N the total number of electrons) towards nucleophiles, electrophiles or radicals, respectively. Condensed Fukui function f_k (Fukui index) is a good intermolecular reactivity descriptor in electrophile–nucleophile (mostly hard-soft) interactions and this has been verified in some cases [70]. It is also considered [71] a reliable descriptor of intramolecular reactivity.

Local electrophilicity ω_k [58, 72] and nucleophilicity N_K [58, 73] have been obtained through a Mulliken Population Atom Spin Density (ASD) analysis of the cation/anion radical formalism of the structures, using $\omega_k = \omega P_k^+$ and $N_k = NP_k^-$ equations.

For the correlation plots, MS Excel and linear regression analysis MS Excel were utilized. Geometry-based parameters have also been computed for the parent congeners *o*-quinone methides **1** and **2** as well as for the nitrosoalkene arm **5** to allow for correlations among the structures. The properties of **8** and **9** were evaluated for their most stable conformers.

Results and discussion

The computationally unveiled features of structures **6** and isomers **7–9**, herein, serve as a model study for this class of compounds. Earlier literature data and our calculations for **1**, **2** and **5** were used in support of our investigation. The credibility of the adopted computational approach (DFT-B3LYP/6−31G** and 6−311++G** as well as MP2/6−311++G**) was tested against alternative functionals and basis sets (see Table 1 and "Methodology" section).

Generation of **6–9**

Structure **6** has been invoked as an intermediate in the oxidative cyclization of benzaldehyde oximes [44, 45]. On the other hand, its benzo-fused analogue **7**, generated similarly, has been trapped by a Diels–Alder self-cycloaddition, and the structure of the resultant spiro adduct-dimer has been confirmed by X-ray analysis [46, 47]. Oximes are known hydrogen donors or acceptors [74, 75]. Computational studies on their *E–Z* geometrical isomers have been reported [76]. The *Z*-conformation of the oxime **I** (Scheme 1) is more stable than its two *E* variants by *ca.* 1.88 kcal mol^{-1}for **6**, *ca.* 1.38 kcal mol^{-1} for **7** and *ca.* 1.7 kcal mol^{-1} for the isomers **8** and **9**. On the other hand, the energy cost for the interconversion of its *E* conformations is *ca.* 4.0 kcal mol^{-1}. Pertinent to the formation of **6** or **7–9** is loss of aromatic character from their precursor oximes **I**, by oxidative dearomatization [77, 78]. This is effected by the overall removal of two σ-electrons from **I** through the collapse of the intermediate complex **II** (Scheme 1) [44, 45].

Energy barriers for the oxidation of **I** to transition states for **6–9** have been calculated (Table 2). In addition, the $E_1 \leftrightarrow E_2$ and $E_1 \leftrightarrow Z$ interconversions, through their corresponding transition states, have low energy demands. The former are of *ca.* 4.3 and 6.6 kcal mol^{-1} for **6** and **7**, respectively, while the latter appear to be more facile with energies of *ca.* 1.4 for **6** and 2.7 kcal mol^{-1} for **7**. However, the $E_2 \leftrightarrow Z$ interconversion is quite an energy-demanding process (*ca.* 30 kcal mol^{-1} for **6** and *ca.* 27–28 kcal mol^{-1} for **7**). Similar trends and magnitudes are observed for the isomers **8** and **9**.

The oxidation process raises the question of identity of the generated intermediate of type III (Scheme 1).The loss of a proton and a hydride ion or two H atoms, sequentially or synchronously lost from II, point to an intermediate of a zwitterionic (**10–21**) or neutral (**6–9**) structure (Fig. 3). If **6–9** are generated directly from the oxime oxidation, then they will assume the conformation of their precursor oxime I. On the other hand, if they take up a *Z* or an *E* conformation, other than that of **I**, then they can only do so through a structure that allows a C_1–C_{10} bond rotation. Structures **10–21**, interconvertible through a H-shift, describe this possibility (Fig. 3). Nitrile oxide **18–21** cannot survive the oxidation conditions. In addition, it is known [79, 80] to dimerize readily to furoxans, and no such reaction has been experimentally confirmed [46–48]. Nevertheless, its transitory existence may be invoked as a short-lived species to mediate energy-allowed interconversions. Apparently, the latter are favoured primarily among **6–9** and their aromatic zwitterions **10–13**, with barriers of *ca.* 9–11 kcal mol^{-1} though mesomeric structures **14–17**, with barriers of *ca.* 12–14 kcal mol^{-1}, may also not be ruled out. The possibility of formation of **22–25**, valence isomers of **6–9** (Fig. 3), was also explored, by analogy to the benzoxete analogue of the parent **1** [81]. Their generation has an energy demand of *ca.* 18 kcal mol^{-1} for **25**, *ca.* 22–23 kcal mol^{-1} for **23** and **24** but a higher one of *ca.* 31 kcal mol^{-1} for **22**. These energy barriers, however, surmountable as they might be, are still up against competing reactions of negligible to very low energy cost, such as the *ortho-* and *peri*-cyclizations actually observed, as has, at present, been experimentally confirmed for **6** and **7** [46–48].

Structure of **6–9**

Dearomatization of **I** imparts a notable distortion onto **6–9** (Tables S2, S3). It is this distortion that absorbs most of the

Scheme 1 Oxime **I** oxidation: commonly proposed route for generation of *o*-quinone methides **III**

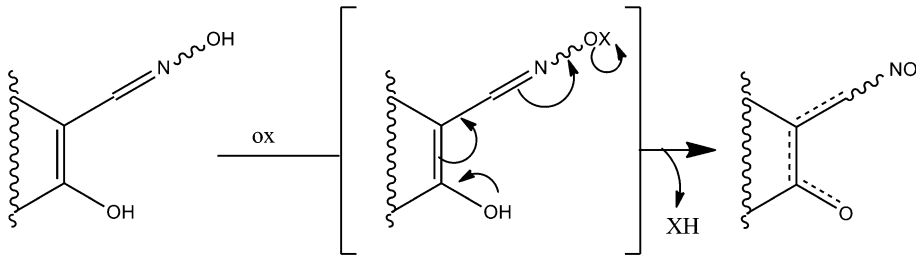

I II III

6-9 and/or **10-13**

ox: $Pb(OAc)_4$, $PhI(OAc)_2$ XH: $Pb(OAc)_2$, PhI, AcOH

Table 2 Relative energies (kcal mol^{-1}) of the minima and transition states (TS) for the $E \leftrightarrow Z$ conformations of **6–9**[a]

Compound	Relative energy
$6E_1$	0
$TS_{6E1-6E2}$	4.2
$6E_2$	−4.3
TS_{6E2-6Z}	30.5
6Z	1.4
$7E_1$	0
$TS_{7E1-7E2}$	1.9
$7E_2$	−6.6
TS_{7E2-7Z}	28.6
7Z	−2.7
$8E_1$	0
$TS_{8E1-8E2}$	2.2
$8E_2$	6.9
TS_{8E2-8Z}	27.6
8Z	−2.9
$9E_1$	0
$TS_{9E1-9E2}$	2.4
$9E_2$	6.7
TS_{9E2-9Z}	28.6
9Z	−3.3

[a] Calculated at the DFT/B3LYP/6−311++G** level of theory

Table 3 Bond lengths (Å), angles (°), and dihedral angles (°) of **I** and **6–9**

	Oximes	6	7	8	9
C_1–$C_{1'}$	1.468[b]	1.426[b]	1.422	1.420	1.416
	1.466[c]	1.361[d]	1.363	1.358	1.356
		1.366[e]	1.369	1.360	1.358
$C_{1'}$–N	1.231	1.323	1.325	1.326	1.321
	1.276	1.412	1.408	1.411	1.407
		1.404	1.407	1.409	1.408
N–O	1.403	1.215	1.212	1.216	1.213
	1.402	1.222	1.224	1.223	1.218
		1.216	1.216	1.215	1.215
C_1–C_2	1.514	1.404	1.389	1.509	1.514
		1.520	1.526	1.520	1.522
		1.520	1.526	1.521	1.523
C_1–$C_{1'}$–$C_{2'}$	133.7	120.5	120.1	120.7	120.4
	121.9	115.7	112.3	116.1	117.2
		117.5	113.5	117.8	118.6
$C_{2'}$–N–O_1	114.8	114.7	115.8	115.6	116.2
	111.2	119.0	121.0	121.7	121.8
		113.5	113.3	114.1	115.2
C_1-$C_{1'}$–$C_{2'}$–N	180	168.0	174.4	174.2	170.2
	180	170.6	154.8	156.1	170.0
		180	172.9	171.4	176.4
C_{10}–C_1–C_2–O_2	138.6	159.2	145.9	146.6	156.6
	140.2	171.9	152.9	152.4	169.8
		180	161.5	161.9	178.7

[a] Calculated at the DFT/B3LYP/6−311++G** level of theory; atoms' positions are the same for all the compounds but atom numbering is shown here for **6–7**. Atom positions follows for **8–9** but atom numbers are different

[b] Z conformation

[c] E conformation

[d] E_1 conformation

[e] E_2 conformation

energy cost incurred during their formation (cf. data of congeners **1** and **2**; Tables S4, S5). The geometry of **6–9** rests largely upon their nitrosoalkene arm. Earlier ab initio calculations [16, 34, 35] on **5** (Table S6) have shown that there is a considerable conjugation between the alkene and the NO group in both conformations, demonstrated by the stretching of the former and contraction of the C–N bond. Indeed, bond lengths of *ca.* 1.420–1.430 Å or 1.480–1.50 Å for the C–C bond in the respective conformations, *ca.* 1.260–1.279 Å for the C–N bond and *ca.* 1.224 Å for the N–O bond have been calculated. The C–C bond length compares well with that of a single sp^2–sp^2 bond (*ca.* 1.480 Å) whereas the C–N bond length resembles that of an imine or oxime (*ca.* 1.280 Å). Remarkably, the NO bond retains its double bond character.

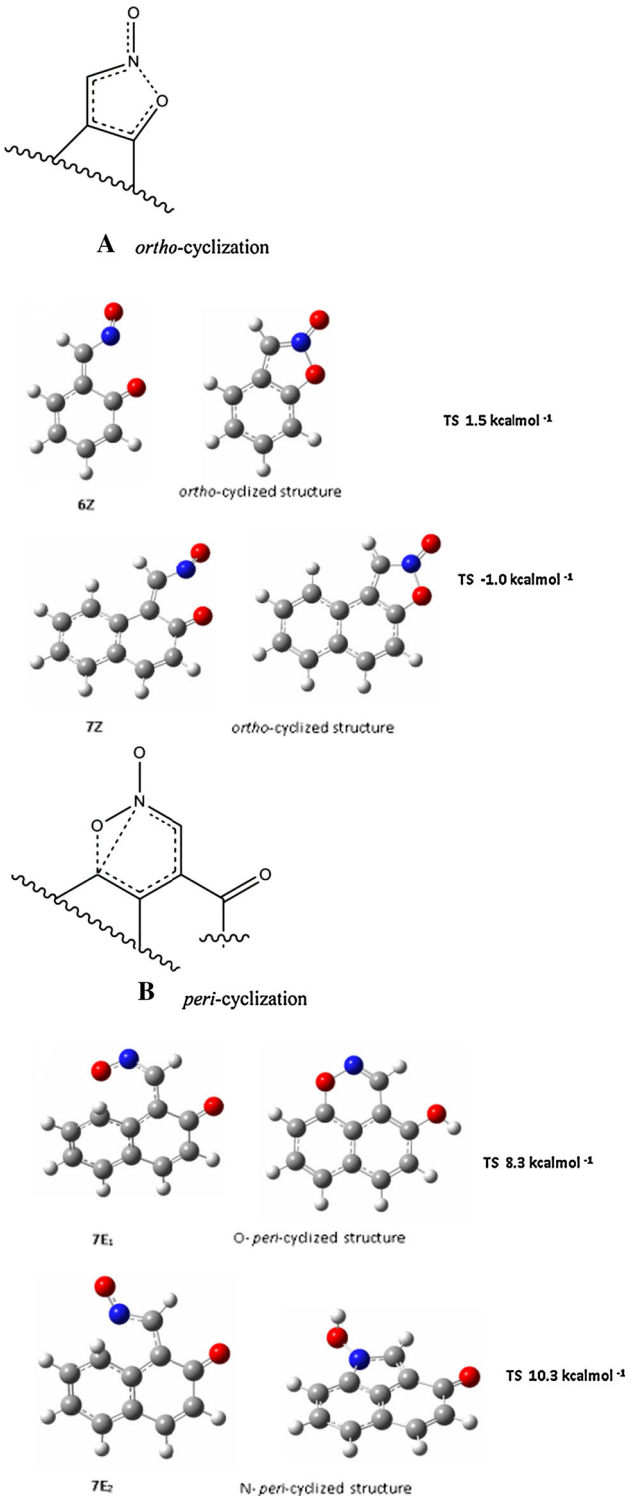

Fig. 4 Geometry-oriented (*Z* or *E* conformers) cyclization modes of **6** and **7**

Table 4 Relative energies of minima and transition states of *ortho*-/*peri*-cyclization of **6** and **7**

Compound	Energy
6Z	1.4
$TS_{6Z\text{-}ortho\text{-}cyclized}$	1.5
"N-oxide"	−16.6
7E1	0
$TS_{7E1-7E2}$	1.9
7E2	−6.6
TS_{7E2-7Z}	28.6
7Z	−2.7
$TS_{7Z\text{-}ortho\text{-}cyclized}$	−1.0
"N-oxide"	−14.0
7E1	0
$TS_{7E1\text{-}peri\text{-}cyclized}$	8.3
a	−4.5
ts_{a-b}	32.5
b	19.3
ts_{b-c}	29.0
c	−25.0
$ts_{c\text{-}product}$	31.6
"1,2-oxazine"	−39.4
7E1	0
$TS_{7E1\text{-}peri\text{-}cyclized}$	8.3
a	−4.5
ts_{a-d}	20.8
d	−9.4
ts_{d-e}	22.9
e	−11.2
ts_{e-f}	17.1
f	−9.2
ts_{f-g}	24.2
g	1.5
ts_{g-h}	25.3
h	2.8
ts_{h-i}	18.8
i	−11.8
$t_{si\text{-}product}$	35.5
"1,2-oxazine"	−39.4
7E1	0
7E2	−6.6
TS_{7E1-j}	10.3
j	1.7
ts_{j-k}	37.4
K	9.7
$ts_{k\text{-}product}$	28.0
"Indole"	−33.3

[a] Calculated using DFT/B3LYP/6−311++G** level of theory

Our calculations (Table S2, Supporting Information, and Table 3) reveal a different geometry for the nitrosoalkene arm of **6–9**. Bond lengths of *ca.* 1.360 Å for C–C and *ca.* 1.323 Å or *ca.* 1.410 Å for C–N bonds in *Z* or *E* conformation, respectively, clearly suggest a rather feeble interaction between the alkenic and the NO unsaturation sites. Accordingly, C–C and N–O bonds are contracted in **6–9**, against their oxime precursors, by *ca.* 0.1Å and

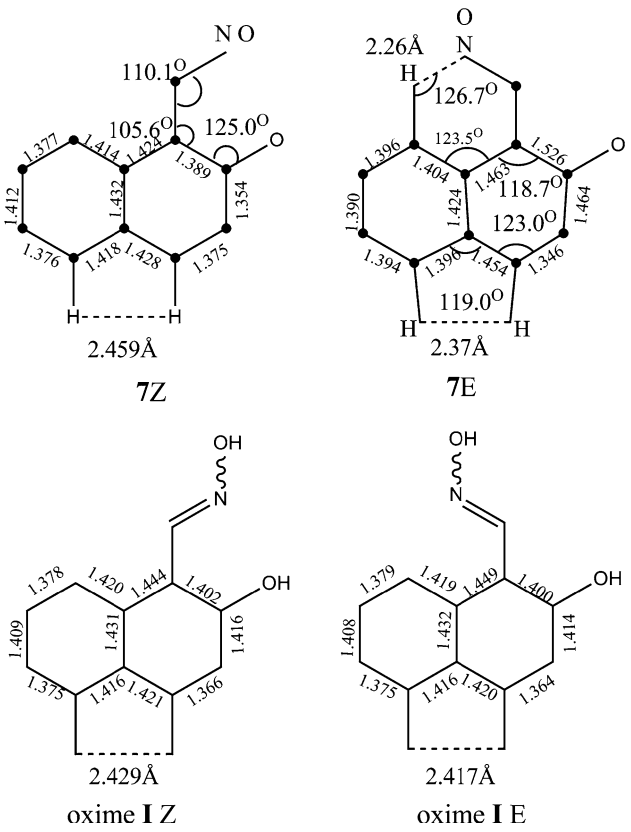

Fig. 5 Conformation-triggered ring σ frame distortion of **7** (compared with oxime **I**)

0.2Å, respectively, accompanied by a slight elongation of the C–N bond by *ca.* 0.1Å, in both their *E* and *Z* conformations. Yet, a weak π polarization is likely to exist in the C–N bond, probably a result of a lone pair effect [82–84], i.e. a repulsive through-space n–π interaction among the N lone pair and the alkene π-orbitals. This, in turn, may be triggered from a similar interaction among the N and O lone pair orbitals of the NO group, reminiscent of the *a*-effect [85–88]. The double bond of the latter, *ca.* 1.223 Å, remains intact, again. In other words, the nitrosoalkene arm retains its two distinct reaction sites (see "Reactivity" section). The NO group is, thus, flexible enough to give rise to the *E or Z* conformations (Fig. 2). **6**–**9** are most stable in their *Z* conformation (Table S3, Supporting Information). Geometry optimization points to a simultaneous cyclization of this conformation in **6** and **7** to a 5-membered "N-oxide ring" whereas their *E* conformers to an "1,2-oxazine" ring or an "indole" ring, respectively (Fig. 4; Table 4).

It is contemplated that bonding interactions develop between the NO group and the exocyclic carbonyl O atom or the π-framework of the benzene core (Fig. 4). For example, a H bonding–like interaction between the NO group and the C-8 (*peri*-) ring hydrogen atom is evident in **7**E_1 and a C–H–N calculated bond length of 2.26 Å and an angle of 126.7° point to this possibility (Fig. 5). Relative energies (Table S3, Supporting information) are consistent with this observation. Similarly, very weak interactions can be inferred for **8** and **9** while such interactions are not found in **6**. These observations have, indeed, been confirmed experimentally [44–47].

Changes more pronounced than those of the ring are observed in the angles of the nitrosoalkene arm (Fig. 6). Thus, the C_1–C_{10}–N angle (φ_2) appears at a steeper orientation by *ca.* 13° in their *Z* conformation while a less sharp but still significant change of C_{10}–N–O (φ_1) of *ca.* 8–10° is found in the *E* conformation. Dihedral angles C_1–C_{10}–N–O_1 and C_{10}–C_1–C_2–O_2 are broader by *ca.* 8–10° in the *E* conformers whereas *Z* ones appear to be virtually unaffected. These data depict the deviation of NO group from alignment with the exocyclic alkene of **7** or **8** [89].

It is important to note, in all cases, the virtually intact double bond character of the NO group whether in the *Z* "N-oxide ring" or the *E* "1,2-oxazine ring", "indole ring" conformations. Similarities are found among the bonding features of the nitrosoalkene arm of **6**, **7** and those of the dinitrosoalkene structure, the well-known intermediate invoked in furoxan isomerization (Table S2, Supporting Information) [90–98]. An intact double bond of *ca.* 1.216–220Å for the NO group is found in both intermediates. However, the C–C bond in the dinitrosoalkene, with a bond length in the range of *ca.* 1.470–1.479Å has been described [30, 99] as an sp^2–sp^2 single bond of a diradical iminoxy-type intermediate, while earlier calculations have indicated a more alkenic bond of 1.321 Å (HF/6−31G*) [69–76] or 1.347–1.392 Å (MP2/6−31G*) [91–98]. That in **6** and **7**, on the other hand, calculated in the range of 1.356–1.420 Å (Table 5), is closer to an alkene, apparently due to the rigidity of their structure as well as their quinone-type stability. In addition, a Diels–Alder self-cycloaddition of **7** to a spiro dimer experimentally confirms the alkenic nature of this bond [46, 47].

The *E* or *Z* conformations also contribute to the distortion of the ring (Fig. 5). Comparing the bond lengths of naphthalene with those calculated for **7**–**9** (Tables S6, S2) demonstrates the impact of the quinone core on the ring distortion, as shown by the notable elongation of both C_1–C_2 and C_1–C_{8a} bonds. The former bond, slightly longer than but still comparable to that in **1** and **2**, ranges from 1.404 to 1.520 Å for **6**, 1.389–1.525 Å for **7** or 1.510–1.522 Å for **8** and **9** (lower end of the ranges refers to the *Z* conformation while the upper end to the *E* conformation). This bond "isolates" the exocyclic alkene from the carbonyl moiety of the quinone segment. The σ-frame distortion is further exemplified by comparing the *E*/*Z* conformation-triggered distortion of oxime **I** with a more marked one in both conformations of **7** (Fig. 5) while

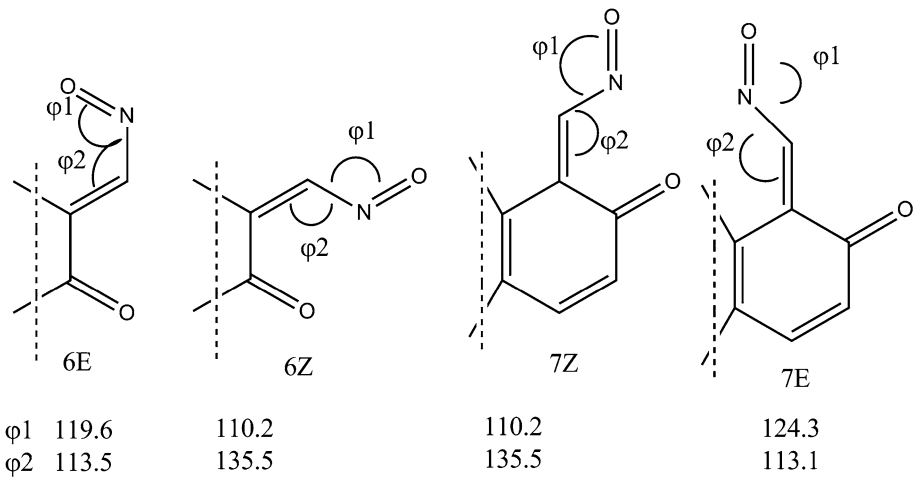

Fig. 6 The *E*/*Z*-conformations of the β -nitroso-*o*-quinone methides **6** and **7**

Table 5 Bond lengths (Å) of exocyclic sites in **1**, **2** and **6–9**

		C–O	C–C	C–N	N–O
1		1.224	1.347		
2		1.224	1.343		
6	*Z*	1.356	1.361	1.418	1.215
	E_1	1.222	1.361	1.407	1.222
	E_2	1.223	1.366	1.408	1.216
7	*Z*	1.354	1.356	1.418	1.212
	E_1	1.221	1.363	1.407	1.224
	E_2	1.220	1.369	1.408	1.216
8	*Z*	1.359	1.358	1.416	1.216
	E_1	1.220	1.368	1.406	1.223
	E_2	1.222	1.363	1.407	1.215
9	*Z*	1.360	1.362	1.415	1.213
	E_1	1.222	1.365	1.408	1.218
	E_2	1.220	1.360	1.407	1.215

Calculated at the DFT/B3LYP/6−311++G** level of theory

similar features with the same trend are observed in **8** and **9**. Accordingly, the *Z* conformation in oxime **I** deforms the structure "outwards", stretching the H–H distance of its *peri* H-4 and H-5 atoms by *ca*. 0.01 Å with respect to its *E* counterpart. A more pronounced change of that H–H distance of *ca*. 0.089 Å is observed among the *E* and *Z* conformers of **7**. More important, however, is the distortion triggered by the dearomatization of oxime **I** to **7**, confirmed by a notable "outward" change of *ca*. 0.03 Å and an "inward" change of *ca*. 0.047 Å of the *peri* H–H distance of their *Z* and *E* conformations, respectively (Fig. 5). These changes are also reflected by changes in the corresponding angles particularly that are formed by the *peri* H-4 and H-5 pseudo-ring.

Much smaller but still noticeable variations, in the range of 0.01–0.02 Å, in the distances of the other H atoms around the structures are also evident. The angular strain [100–102], thus, introduced, causes some bond alternation (bond localization) in the benzene ring (SIBL effect) [103–105]. The benzene bond length variation ranges from *ca*. 0.005–0.02Å in the *E* conformations of **7**, *ca*. 0.006–0.01 Å in **8**, *ca*. 0.02–0.04 Å in the *Z* conformation of **7** and *ca*. 0.01–0.06 Å in **9**. Its average bond length is 0.001 Å in **7** or **8** and 0.005 Å in **9** longer than the commonly accepted values of 1.399 Å or 1.402 Å for the isolated structures of benzene or naphthalene, respectively [106]. The bond length variation range shows that (a) *E* conformation is less strained, (b) the carbocycle is more aromatic in **7** and **8** *E* conformers and (c) the carbocycle and the quinone part are more or less isolated from each other, to a greater extent in **7** and **8**.

The exocyclic isomer pattern in **7–9** also perturbs their σ/π-framework. In the 1,2-pattern, as in **7** and **8**, the energy cost will be that corresponding to the resonance energy of naphthalene less that of benzene. The 2,3-pattern, as in **9**, however, costs the whole resonance energy of naphthalene for its formation, thus, it is expected to be unstable, highly reactive though energetically and geometrically capable of

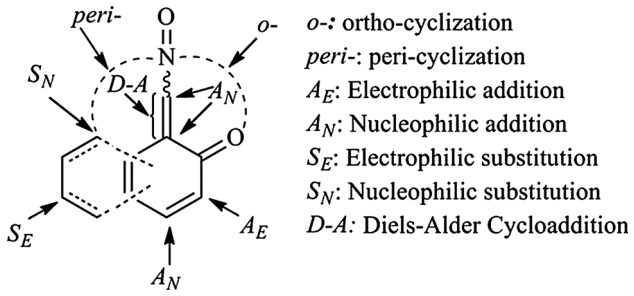

Fig. 7 Reactivity profile of **6–9**

existence. Some double bond character observed in C_2–C_3, C_4–C_{4a} and C_1–C_{8a} indicates a weak π delocalization throughout the ring structures. Bond length variations (Δ_R) in the aromatic part of the *E* conformations of **7** (Fig. 5; Table S2) or the *Z* conformation of **8** support this observation and point to a *peri-* (Fig. 4b) or an *ortho*-annelated (Fig. 4a) ring structure, respectively, as mentioned earlier. On the other hand, Δ_R values of *ca.* 0.01–0.07 for **6** or *ca.* 0.01–0.06 for **9** (Table S2) are indicative of the substantial diene character of these rings. The distortion profile of **6–9**, as detailed above, could safely point to these structures as a satisfactory description of a rather late (product-like) transition state in the oxidative dearomatization process (Scheme 1).

Reactivity profile of **6–9**

Features that dominate a structure invariably accompany or match those that dictate its reactivity. The latter refers to the kinetic control of a reaction and depends on reactant energies, energies of transition states and/or intermediates leading to stable products. Probing the electron distribution and its perturbation by changes in the structures of **6–9** allows one to detect ultimately a reactivity pattern for them [107]. To that end, in addition to the geometric parameters used above, the following reactivity descriptors were computed. Values of notable magnitude and variation, obtained for the chemical potential μ and dipole moments (obtained as the sum of σ and π contributions) of **6–9** (Table S7), exemplify their electrophilic character [59, 60].

Further, the HO (also HO-1) and LU (also LU + 1) molecular orbitals (Figs. S1 and S2, Supporting Information) of **6–9** are found to be localized on the ring core and the nitrosoalkene arm, respectively. The energies and separation of these orbitals (HOMO–LUMO gap) [63] (Fig. S3 and Table S8 in Supporting Information) are seriously affected by the *E*- and *Z*-conformation of **6** and **7** (or **8** and **9**). The HO-1 orbital is the most affected one, as that being the most strongly related to π delocalization [61, 62], due to the electron-withdrawing character of the NO group. This distribution points to a ring core susceptible towards both nucleophiles and electrophiles and a nitrosoalkene arm susceptible towards nucleophiles (Fig. 7).

Mulliken charges [61, 62] (Table S9) and Fukui f(r) [67, 68] (Table S10) values also consistently indicate the nitrosoalkene arm as the major site for a nucleophilic attack. Parr electro (nucleo) philicity indices, ω_k and N_K (Tables S11, S12), on the other hand, while following a similar trend, they introduce some additional features. These predictions indicate a general pattern that bears a good analogy to the observed reactivity of **1** or **2** with O and N nucleophiles [22].

Indeed, Fukui values of **6–8**, in both *E* and *Z* conformations, suggest a site selectivity of the structure towards electrophiles localized on the NO group, barely indicating alternative positions. Parr data (N_K), on the other hand, feebly support electrophilic addition primarily at C-1 and to a lesser extent at C-3 or electrophilic substitution at C-4 and C-6. On the contrary, Fukui values appear to favour electrophilic addition in **9**, primarily at C-1 and C-4 and virtually all positions of the fused ring to a lesser extent, whereas no comparable sensitivity is exhibited by Parr values. These estimates are in line with geometry parameters of **9** and lend support to its diene character. While predictions for the *E* conformation of **6** and **9** may be reasonable, the low sensitivity of both descriptors towards electrophiles of the *Z* conformation of **6** as well as the rest of the structures in both conformations cannot be readily rationalized, given their propensity to cyclise. However, site susceptibility towards nucleophiles appears to follow a general trend by both descriptors. Thus, it engages the α,β-unsaturation sites, primarily that of the nitrosoalkene arm, in a nucleophilic Michael-type addition in both *E* and *Z* conformations. This susceptibility demonstrates (a) the diene geometry of the quinone ring, (b) the localized alkene character of the nitrosoalkene arm (cf. Fukui data of **5**, Table S10) and (c) the partial polarization of the fused ring relayed by the quinone one. These reactivity patterns, however, are corroborated only in part by experimental results [22, 46, 47, 49]. Of interest is the lack of sensitivity of the indices towards substitution (electrophilic or nucleophilic) reactivity. Of course, one should keep in mind (a) calculations refer to an isolated molecule, (b) the dependence of site selectivity upon the reaction surroundings (i.e. solvent effects and reagent interactions), particularly in a substitution reaction.

It can be safely argued that intramolecular (*o-* or *peri-*) cyclization is the prevalent reaction course (apparently the kinetically controlled one) and takes precedence over any other reaction, even in the presence of an external stimulus (a nucleophile or an electrophile, as also suggested by structural data, see "Structure" section). In the event, the dual character of the NO group (as an electrophile or a

nucleophile), probably enhanced by the lone pair repulsion among NO orbitals, [84–88] (see "Structure" section) and the low rotation barrier between the *E* or *Z* conformations (see "Structure" section and Fig. 3), apparently have a decisive impact on their predicted reactivity profiles.

The aromatic character and its geometry-triggered variation, as an additional probe for the reactivity of **6–9** as well as that of their precursor oximes **I**, have also been examined by means of the HOMA [62, 64] (Table S13) and π delocalization-sensitive deformation energy (E_{def}) [65, 66] (Table S13) descriptors.

HOMA values of the *E* conformer of **I** are higher than those of its *Z* conformer. This is attributed to a 6-membered pseudo-ring formed by intramolecular Resonance-Assisted Hydrogen Bonding (RAHB leitmotif) [108] in the *Z* conformer, which perturbs the ring π density, causing a drop of aromaticity [109–111]. The latter builds up in going from **I** to **6–8** in their *Z* conformation and decreases in moving to **9**. It falls drastically in the E_2 conformation of **7–9** whereas it is lost in the *E* conformations of **6**. Loss of aromaticity in the *E* conformation of **6** drives the structure to a non aromatic diene geometry. Its increase, on the other hand, in the *Z* conformation of **6** or **7** and **8** is consistent with the ring angular *ortho*-annelation (see earlier "Discussion" and Fig. 4a). The latter develops an extended π delocalization throughout the entire structure [109–111]. This rationale can also account for the lower values of the *E* conformations of **7**, pointing to a *peri* (1,8)-ring annelation (Fig. 4b). The drop in **9** is attributed to the outer ring diene geometry of the linearly annelated tricycle. E_{def} (Table S13) also shows a ring annelation trend as reflected by the higher values estimated for the *Z* conformation in **6** or the *E* conformation in **7**.

Plots of aromaticity-related hardness η [61, 62] (Fig. S4, $R^2 = 0.587$, Table S7) or HOMO–LUMO gap [63]

(Fig. S3, $R^2 = 0.536$, Table S8) against HOMA drawn. Both demonstrate a poor linear correlation, reflecting, and confirming the weak impact of ring stability (i.e. reactivity related to ring distortion) on π interactions. However, a satisfactory linear correlation ($R^2 = 0.859$) of HOMA against activation energy ($\Delta G^{\ddagger}$) is obtained (Fig. S5). This correlation supports the stabilizing effect of the *ortho*-ring formation on the *Z* conformation and to a much lesser extent that of a *peri*-ring formation on the *E* conformation.

The impact of the *E* or *Z* conformation on the ring stability is evident, once again. Indeed, the *Z* conformation has a more extended π delocalization (more stable) while a more Clar-type formulation [112] describes the *E* conformation, particularly in **7** and **8**. A detailed account on the features pertaining to the intramolecular *ortho*- and *peri*-cyclization of **6** and **7**, along with substituent and reaction medium effects on its mechanism, will be reported in due course.

Conclusions

β-Nitroso-*o*-quinone methides **6–9** are highly reactive species with a notably distorted geometry. Their nitrosoalkene arm gives rise to *E* and *Z* conformations. The *E* or *Z* conformations, the *o*-quinone ring, the 1,2-(**7** and **8**) or 2,3- (**9**) isomer pattern and their corresponding angular or linear ring formations contribute to the σ-frame-based, mainly, ring distortion. The *ortho*-(angular or linear) or *peri*-ring formations stabilize the *Z* or *E* conformers, respectively.

Geometry and reactivity descriptors depict a versatile reactivity pattern, dictated by the nitrosoalkene arm, the quinone ring and the benzene ring (Clar-type or diene-geometry), as virtually individual entities. This is displayed on the ring and the nitrosoalkene arm. The prevalent reaction is an intramolecular *ortho*- or *peri*-cyclization, through the NO group of the nitrosoalkene arm. Further, the former or both may be geometry-controlled primary processes. The NO group unveils a dual reactivity profile, as an electrophile (*ortho*-cyclization mode) or as a nucleophile (*peri*-cyclization mode). Intermolecular primary reaction types and ring susceptibility sites towards electrophiles or nucleophiles are predicted as mainly electrophilic or nucleophilic additions. These predictions are partly experimentally confirmed. The nitrosoalkene arm is highly prone to nucleophilic attack (at the carbon directly bonded to NO group) by virtue of its geometry, its propensity to convert to its oxime stable tautomer and to trigger the ring rearomatization (i.e. "revert to type" aromatic stability).

Both Fukui and Parr functions seemed to be, in general, of comparable credibility. Discrepancies of both descriptors with experimental findings, mainly in reference to substitution reactivity, are attributed to the proclivity of the structure towards intramolecular reactivity. The predictions are en bloc indicative of the strongly electrophilic character of **6–9**.

Clearly, the structure and reactivity profile of **6–9** demonstrates the potential of these structures to provide efficient access to a diverse array of useful molecular scaffolds for a target-oriented pipeline drug discovery and design.

Acknowledgments The authors thank Professor G. Varvounis for useful comments on aspects of the work.

References

1. Rokita SE (2009) Quinone methides. Willey, Hoboken
2. VandeWater RW, Pettus TRR (2002) Tetrahedron 58:5367–5405

3. Chen MW, Cao LL, Ye ZS, Jiang GF, Zhou YG (2013) Chem Commun 49:1660–1662
4. Willis NJ, Bray CD (2012) Chem Eur J 18:9160–9173
5. Wang H, Wahl MS, Rokita SE (2008) Angew Chem Int Ed 47:1291–1293
6. Sharma A, Santos IO, Gaur P, Ferreira VE, Garcia CRS, da Rocha DR (2013) Eur J Med Chem 59:48–53
7. Han I, Russell DJ, Kohn H (1992) J Org Chem 57:1799–1807
8. Tomasz M, Das A, Tang KS, Ford MGJ, Minnock A, Musser SM, Waring MJ (1998) J Am Chem Soc 120:11581–11593
9. Angle SR, Rainier JD, Woytowicz C (1997) J Org Chem 62:5884–5892
10. Angle SR, Yang WJ (1992) J Org Chem 57:1092–1097
11. Gaudiano G, Frigerio M, Bravo P, Koch TH (1990) J Am Chem Soc 112:6704–6709
12. Li TH, Rokita SE (1991) J Am Chem Soc 113:7771–7773
13. Zeng QP, Rokita SE (1996) J Org Chem 61:9080–9081
14. Pande P, Shearer J, Yang JH, Greenberg WA, Rokita SE (1999) J Am Chem Soc 121:6773–6779
15. Rokita SE, Yang JH, Pande P, Greenberg WA (1997) J Org Chem 62:3010–3012
16. Yang BY, Zollner T, Gebhardt P, Mollmann U, Miller MJ (2010) Org Biomol Chem 8:691–697
17. Amouri H, Besace Y, Le Bras J, Vaissermann J (1998) J Am Chem Soc 120:6171–6172
18. Amouri H, Le Bras J (2002) Acc Chem Res 35:501–510
19. Amouri H, Vaissermann J, Rager MN, Grotjahn DB (2000) Organometallics 19:1740–1748
20. Amouri H, Vaissermann J, Rager MN, Grotjahn DB (2000) Organometallics 19:5143–5148
21. Chiang Y, Kresge AJ, Zhu Y (2000) J Am Chem Soc 122:9854–9855
22. Shaikh AK, Cobb AJA, Varvounis G (2012) Org Lett 14:584–587
23. Di Valentin C, Freccero M, Zanaletti R, Sarzi-Amade M (2001) J Am Chem Soc 123:8366–8377
24. Angle SR, Arnaiz DO, Boyce JP, Frutos RP, Louie MS, Mattsonarnaiz HL, Rainier JD, Turnbull KD, Yang WJ (1994) J Org Chem 59:6322–6337
25. Taing M, Moore HW (1996) J Org Chem 61:329–340
26. Katritzky AR, Zhang ZX, Lan XF, Lang HY (1994) J Org Chem 59:1900–1903
27. Dell CP (1998) J Chem Soc Perkin Trans 1:3873–3905
28. Tietze L, Kettschau G (1997) In: Metz P (ed) Topics in current chemistry. Springer, Berlin, pp 1–120
29. Basaric N, Doslic N, Ivkovic J, Wang YH, Malis M, Wan P (2012) Chem Eur J 18:10617–10623
30. Bentley TW (2011) Org Biomol Chem 9:6685–6690
31. Chiang Y, Kresge AJ, Zhu Y (2001) J Am Chem Soc 123:8089–8094
32. Chiang Y, Kresge AJ, Zhu Y (2002) J Am Chem Soc 124:717–722
33. Modica E, Zanaletti R, Freccero M, Mella M (2001) J Org Chem 66:41–52
34. Bodnar BS, Miller MJ (2011) Angew Chem Int Ed Engl 50:5629–5646
35. Gowenlock BG, Richter-Addo GB (2005) Chem Soc Rev 105:797–809
36. Lyapkalo IM, Ioffe SL (1998) Russ Chem Rev 67:467–484
37. Tsoungas PG (2002) Heterocycles 57:1149–1178
38. Tsoungas PG (2002) Heterocycles 57:915–953
39. Wieser K, Berndt A (1975) Angew Chem Int Ed Engl 14:70–71
40. Francotte E, Merenyi R, Vandenbulckecoyette B, Viehe HG (1981) Helv Chim Acta 64:1208–1218
41. Smith JH, Heidema JH, Kaiser ET (1972) J Am Chem Soc 94:9276–9277
42. Veronese AC, Vecchiati G, Sferra S, Orlandini P (1985) Synthesis 300–302
43. Kwiatkowski M, Kwiatkowski E, Olechnowicz A, Ho DM, Deutsch E (1990) J Chem Soc Dalton Trans 2497–2502
44. Boulton AJ, Tsoungas PG (1980) J Chem Soc Chem Commun 421–422
45. Boulton AJ, Tsoungas PG, Tsiamis C (1986) J Chem Soc Perkin Trans 1:1665–1667
46. Supsana P, Tsoungas PG, Aubry A, Skoulika S, Varvounis G (2001) Tetrahedron 57:3445–3453
47. Supsana P, Tsoungas PG, Varvounis G (2000) Tetrahedron Lett 41:1845–1847
48. Dolka C, Van Hecke K, Van Meervelt L, Tsoungas PG, Van der Eycken EV, Varvounis G (2009) Org Lett 11:2964–2967
49. Liaskopoulos T, Skoulika S, Tsoungas PG, Varvounis G unpublished results
50. Smith JA, Le Q, Jones ED, Deadman J (2010) Future Med Chem 2:215–224
51. Ikeda R, Kuwano R (2012) Molecules 17:6901–6915
52. Zhao Y, Truhlar DG (2008) Acc Chem Res 41:157–167
53. Simón L, Goodman JM (2011) Org Biomol Chem 9:689–700
54. Woon D, Dunning TH Jr (1995) J Chem Phys 103:4572–4585
55. Valiev M, Bylaska EJ, Govind N, Kowalski K, Straatsma TP, Van Dam HJJ, Wang D, Nieplocha J, Apra E, Windus HJJ, de Jong W (2010) Comput Phys Commun 181:1477–1489
56. Sloot PA, Abramson D, Bogdanov A, Gorbachev Y, Dongarra J, Zomaya A, Black G, Schuchardt K, Gracio D, Palmer B (2003) Computational science ICCS. Springer, Berlin, pp 122–131
57. Shao Y, Molnar LF, Jung Y, Kussmann J, Ochsenfeld C, Brown ST, Gilbert ATB, Slipchenko LV, Levchenko SV, O'Neill DP, DiStasio RA Jr, Lochan RC, Wang T, Beran GJO, Besley NA, Herbert JM, Yeh Lin C, Van Voorhis T, Hung Chien S, Sodt A, Steele RP, Rassolov VA, Maslen PE, Korambath PP, Adamson RD, Austin B, Baker J, Byrd EFC, Dachsel H, Doerksen RJ, Dreuw A, Dunietz BD, Dutoi AD, Furlani TR, Gwaltney SR, Heyden A, Hirata S, Hsu CP, Kedziora G, Khalliulin RZ, Klunzinger P, Lee AM, Lee MS, Liang W, Lotan I, Nair N, Peters B, Proynov EI, Pieniazek PA, Min Rhee Y, Ritchie J, Rosta E, Sherrill CD, Simmonett AC, Subotnik JE, Lee Woodcock E III, Zhang W, Bell AT, Chakraborty AK, Chipman DM, Keil FJ, Warshel A, Hehre WJ, Schaefer AK III, Kong J, Krylov AI, Gill PMW, Head-Gordon M, (2006) Phys Chem Chem Phys 8:3172–3191
58. Domingo LR (2013) RSC Adv 3:1486–1494
59. Domingo LR, Perez P, Contreras R (2004) Tetrahedron 60:6585–6591
60. Perez P, Domingo LR, Burell AJ, Contreras R (2003) Tetrahedron 59:3117–3125
61. Alonso M, Herradon B (2010) J Comput Chem 31:917–928
62. Poater J, Duran M, Sola M, Silvi B (2005) Chem Rev 105:3911–3947 and references cited therein
63. Pearson RG (1993) Acc Chem Res 26:250–255
64. Raczyńska ED, Hallman M, Kolczyńska K, Stępniewski TM (2010) Symmetry 2:1485–1509
65. Shishkin OV, Omelchenko IV, Krasovska MV, Zubatyuk RI, Gorb L, Leszcynski J (2006) J Mol Struct 791:158–164
66. Zhigalko MV, Shishkin OV, Gorb L, Leszcynski J (2004) J Mol Struct 693:153–159
67. Gonzalez-Suarez M, Aizman A, Soto-Delgado J, Contreras R (2012) J Org Chem 77:90–95
68. Fuentealba P, David J, Guerra D (2010) J Mol Struct: THEOCHEM 943:127–137
69. Pilepić V, Uršić S (2001) J Mol Struct:THEOCHEM 538:41–49
70. Roy RK, Usha V, Pauloviè J, Hirao K (2005) J Phys Chem A 109:4601–4606

71. Chattaraj PK, Sarkar U, Roy DR (2006) Chem Rev 106:2065–2091
72. Chattaraj PK, Giri S, Duley S (2011) Chem Rev 111:43–75
73. Pratihar S, Roy S (2010) J Org Chem 75:4957–4963
74. Mikhaleva AI, Zaitsev AB, Trofimov BA (2006) Usp Khim 75:884–912
75. Pratt DA, Blake JA, Mulder P, Walton JC, Korth HG, Ingold KU (2004) J Am Chem Soc 126:10667–10675
76. Xu WR, Wang JW, Liu CB, Chen CL (2004) J Chin Chem Soc-Taip 51:1259–1266
77. Pouysegu L, Deffieux D, Quideau S (2010) Tetrahedron 66:2235–2261
78. Roche SP, Porco JA (2011) Angew Chem Int Edit 50:4068–4093
79. Pasinszki T, Westwood NPC (2011) Curr Org Chem 15:1720–1733
80. Yu ZX, Caramella P, Houk KN (2003) J Am Chem Soc 125:15420–15425
81. Meier H (2012) Molecules 17:1548–1570
82. McCarrick MA, Wu YD, Houk KN (1992) J Am Chem Soc 114:1499–1500
83. McCarrick MA, Wu YD, Houk KN (1993) J Org Chem 58:3330–3343
84. Perakyla M (1996) J Org Chem 61:7420–7425
85. Buncel E, Um IH (2004) Tetrahedron 60:7801–7825
86. Fountain KR, Tad-y DB, Paul TW, Golynskiy MV (1999) J Org Chem 64:6547–6553
87. Um IH, Buncel E (2000) J Org Chem 65:577–582
88. Um IH, Lee JS, Yuk SM (1998) J Org Chem 63:9152–9153
89. Rauhut G, Eckert F (1999) Sci Prog 82:209–231
90. Bird CW (1997) Tetrahedron 53:3319–3324
91. Eckert F, Rauhut G (1998) J Am Chem Soc 120:13478–13484
92. Eckert F, Rauhut G, Katritzky AR, Steel PJ (1999) J Am Chem Soc 121:6700–6711
93. Rauhut G (2001) J Org Chem 66:5444–5448
94. Chiari G, Viterbo D (1982) Acta Crystallogr B 38:323–325
95. Friedrichsen W (1994) J Phys Chem 98:12933–12937
96. Ponder M, Fowler JE, Schaefer HF III (1994) J Org Chem 59:6431–6436
97. Rauhut G (1996) J Comput Chem 17:1848–1856
98. Seminario JM, Concha MC, Politzer P (1992) J Comput Chem 13:177–182
99. Yu Z-X, Caramella P, Houk KN (2003) J Am Chem Soc 125:15420–15425
100. Siegel JS (1994) Angew Chem Int Ed Engl 33:1721–1723
101. Stanger A, Ben-Mergui N, Perl S (2003) Eur J Org Chem 2709–2712
102. Stanger A, Boese R, Ashkenazi N, Stellberg P (1998) J Organomet Chem 556:249–250
103. Bao P, Yu ZH (2007) J Phys Chem A 111:5304–5313
104. Rappoport Z, Kobayashi S, Stanger A, Boese R (1999) J Org Chem 64:4370–4375
105. Stanger A, Tkachenko E (2001) J Comput Chem 22:1377–1386
106. Krygowski TM, Cyranski MK (2003) Synlett 1570–1570
107. Garza J, Vargas R, Aquino N, Sen KD (2005) J Chem Sci 117:379–386
108. Gilli P, Pretto L, Bertolasi V, Gilli G (2009) Acc Chem Res 42:33–44
109. Feixas F, Matito E, Poater J, Sola M (2007) J Phys Chem A 111:4513–4521
110. Palusiak M, Simon S, Sola M (2006) J Org Chem 71:5241–5248
111. Poater J, Fradera X, Duran M, Sola M (2003) Chem Eur J 9:1113–1122
112. Portella G, Poater J, Sola M (2005) J Phys Org Chem 18:785–791